Modeling electricity consumption using nighttime light images and artificial neural networks

Tomasz Jasiński*

Faculty of Management and Production Engineering, Łódź University of Technology, Piotrkowska 266, 90924 Łódź, Poland

* Corresponding author.
E-mail address: tomasz.jasinski@p.lodz.pl

Declarations of interest: none

Role of the funding source. The Łódź University of Technology financed the proofreading of the article by a native English speaker with expertise in the field.

Abstract

The purpose of this paper is to model electricity consumption using Artificial Neural Networks (ANN). Total electricity consumption and consumption generated by households (HH) were modeled. The input variables of the ANN were based on nighttime light images from VIIRS DNB. Studies conducted thus far have covered mainly linear models. Most of case studies focused on single countries or groups of countries with only few focusing on the sub-national scale. This paper is pioneering in covering an area of Poland (Central Europe) at NUTS-2 level. The use of ANN enabled the modeling of the non-linear relations associated with the complex structure of electricity demand. Satellite data were collected for the period 2013–2016, and included images with improved quality (inter alia higher resolution), compared to the DMSP/OLS program. As images are available from April 2012 onwards, it is only recently that their number has become sufficient for ANN learning. The images were used to create models of multilayer perceptrons. The results achieved by ANN were compared with the results obtained using linear regressions. Studies have confirmed that electricity consumption can be determined with higher precision by the ANN method.

Keywords: electricity consumption; nighttime light images; artificial neural networks

JEL: Q41, O13, C45

1. Introduction

Electricity is a fundamental determinant of quality of life in modern society. Sustainable development in the field of energy requires knowledge of both the demand and supply side of the market. A significant part of electricity is consumed for lighting (and other purposes that produce visible light). The effects of such human activities are observable not only on Earth, but also beyond it. Orbiting satellites continuously observe the globe and record images. The sheer number of satellites and their sensors results in a variety of available data. These include nighttime light images developed and made available by The Earth Observations Group (EOG) at National Centers for Environmental Information (NOE) of the National Oceanic and Atmospheric Administration (NOAA). Publicly available data from the US Air Force Defense Meteorological Satellite Program (DMSP) Operational Linescan System (OLS) cover the period between 1992 and 2013. As of April 2012, more detailed nighttime light images from the Visible Infrared Imaging Radiometer Suite (VIIRS) Day/Night Band (DNB) are available (see Fig. 1). These are used to monitor human activities and their impact on the environment. In particular, activities and the economic state of the population are analyzed, e.g. by modeling Gross Domestic Product (GDP) [1,2,3,4,5], its dynamics [6] and accuracy (assuming that it is misleading or biased) [7] or poverty level [8], as well as population numbers [9] and its density [10,11,12], seasonal population [13] and electricity consumption (more in [14]). In most studies mentioned here the authors use linear (e.g.

[1,2,6,8,9]), logarithmic (e.g. [3] – decimal logarithm, [4] – natural logarithm), quadratic polynomial [6], power function [6,7] and exponential [7] regression models to describe the relations in question.

Fig. 1. Fragment of a night-light image from VIIRS DNB (part of Europe, December 2016).
Source: NOE/NOAA.

Based on NOE/NOAA data, Ghosh et al. [1] carried out a comparison between human well-being and electrification rates. The relation between the brightness of nighttime lights and electricity consumption is obvious. As Addison and Steward rightly pointed out [15], according to IEA/OECD 2006, only 1% of lighting is based directly on burning fuels (not on electricity). While the nature of the relation between nighttime light intensity and electricity consumption for street lighting appears to be evident and well-established [16], the issue is more complex in the case of total energy demand due to the complex structure of demand itself. For example, street lighting (e.g. in road intersections) does not translate into the electricity consumption of households (HH). Rossi et al. [17] indicate the impact of lighting bulb types in use (e.g. LED, CMH lamps) on electricity consumption, and the flux degradation of an LED with time due to thermal and mechanical stress. In specific cases, this means that the time factor should be taken into account in the analyses carried out. The consumption of electricity in highly industrialized areas (concentration of production companies) is different than in other areas, e.g. with a predominance of residential buildings (a different pattern of energy consumption in these areas has been pointed out by i.e. To et al. [18] on the basis of empirical studies). Differentiation of electricity consumption can also be expected within HH. While the amount of electricity used for lighting purposes is relatively constant, other applications depend on many factors, including income (the eastern part of Poland is a less economically developed area than the rest of the country), the age structure of the population [19] and the method of heating (e.g. electricity, fossil fuels etc.). Hu et al. [20] presented an international comparison of final energy consumption per floor area. Among the countries surveyed, Chinese urban areas (excluding northern urban heating energy use) exhibited the lowest value of index (49 kWh/m^2) and Russia the highest (384 kWh/m^2). These values differ from each other almost eight times clearly indicating the different patterns of energy consumption by households in different regions of the world.

For these reasons, it can be assumed that relation between nighttime light intensity and total electricity consumption is not linear (especially for analyses covering a number of economically different areas). This assumption is in line with the results of earlier studies. Tripathy et al. [21] pointed out that the brightest areas could indicate both the most populated and most industrial areas (e.g. 24-hour power plants), for which the structure and volume of electricity consumption are different. Analyses conducted on the basis of nighttime light images, although usually

The final version is available on the journal website at https://doi.org/10.1016/j.energy.2019.04.221

covering entire countries (Xie and Weng [22] – worldwide; Shi et al. [23] – initially Japan, and then worldwide, excluding countries for which data were not available; Shi et al. [24] – countries along the Belt and Road; Elvidge et al. [25] – 21 countries; He et al. [26] and Xie and Weng [27] – Mainland China; Ramdani and Setiani [28] – Indonesia), can be broken down to smaller parts. Doll et al. [29] have studied areas between NUTS-1 and NUTS-3, Letu et al. [30] 11 selected regions in Japan, and Shi et al. provinces and prefectures level in China [31].

Fehrer and Krarti [32] used linear regression to build a model of electricity consumption for buildings in 49 regions in the USA. For this purpose, they used the total night lights (TNL) defined according to Eq. 1.

$$TNL = \sum_{k=1}^{K}(L_k \times \frac{A_k}{A_R}) \quad (1)$$

where: K – number of pixels, L_k – total radiation measured in pixel no. k, A_k – area covered with k-th pixel, A_R – reference area of a 15 arc-second pixel at the equator (463 m × 463 m).

Previously, the TNL index has been used inter alia by Shi et al. [31].

It should be noted that there are alternative indicators of the amount of light in satellite images. In order to define regional economic development, Li et al. [33] used the sum of lights (SOL) defined as:

$$SOL = \sum_{i=1}^{B_{max}}(N_i \times B_i) \quad (2)$$

where: N_i – number of pixels with value i (images are in grey scale, so every RGB component has equal value as i), B_i – brightness value, B_{max} – maximum pixel value in the image.

An similar approach was applied by Jing et al. [34], who additionally introduced the threshold value. Pixels with lower values were not summed.

Further, Reza and Chasovskich [35] defined the compounded night-light index (CNLI):

$$CNLI = {}^{1}/_{N_L \times B_{max}} \times \sum_{i=B_0}^{B_{max}}(N_i \times B_i) \quad (3)$$

where: B_0 – cut-off point (minimum value of pixels used in calculations), N_L – number of pixels with values in the range $[B_0,B_{max}]$. The remaining variables were defined as in Eq. 2.

The approaches presented above enable the calculation of total radiation. They do not afford the option to divide radiation into ranges by intensity, and do not allow for the averaging of results using many images. For the purposes of this paper, it was necessary to develop such a method.

Attention should be paid to the study by Wang et al. [36], in which they demonstrated the high sensitivity of nighttime light images to the change of aerosols. By creating a model of linear regression, they linked the brightness of images with the concentration of surface particulate matter with aerodynamic diameters less than 2.5 mm (PM2.5). The research covered the area of Atlanta (Georgia, USA) in the period August–October 2012. The presence of the described relations was confirmed by Fu et al. [37] in research conducted in Beijing (China). Based on the results of these studies, it should be noted that in the case of places with sudden changes in PM2.5, the brightness of pixels may differ to some extent from the actual radiation emitted in this area. When creating a model, it is necessary to bear in mind the risk of malfunctioning caused by this phenomenon, especially if the research has a long span of time.

Studies have identified that **there are at least two knowledge gaps when it comes to analyzing new images from the VIIRS DNB.** The first concerns the use of Artificial Intelligence (AI) tools for the non-linear modeling of electricity demand. The available test results are mostly based on data from the previous DMSP/OLS program with different image parameters, and do not use AI. The most commonly used linear regression in analyses, as indicated by R^2 values (e.g. from 0.1832 to 0.8961 in [32] and from 0.9094 to 0.9305 in [30]), is not able to explain fully the existing relations in studies covering smaller regions and not entire countries. Non-linear analyses – particularly those based on AI – have the ability to model at a much more advanced level and with fewer errors. An often observed advantage of AI (in particular ANN) to other techniques is related to the principles of its function, described in section 2. More specifically, it concerns the ability of ANN to search in a highly automated way for non-linear (often complex) relations between independent and dependent variables. Modeling does not require full knowledge of the type

The final version is available on the journal website at https://doi.org/10.1016/j.energy.2019.04.221

and parameters of a relation, which in combination with the automation provided by ANN enables the discovery of previously unknown dependencies between variables. Thus, they provide an opportunity to improve the results achieved by models developed thus far. While these methods are widely used in many other areas related to the electricity market, there is a clear research gap as far as modeling based on satellite nighttime images is concerned. **The number of publications covering the modeling of electricity consumption with AI (including ANN) based on nighttime light images in both the Scopus and Web of Science databases was zero as of August 24, 2018.**[1] The second knowledge gap concerns the lack of research conducted at the regional level for Eastern European countries. Global analyses are interested in entire countries and, hence, do not take into account local differences within a given country. As the modeled relations are connected, among others, with economic, social and environmental factors, they differ from the countries analyzed so far in other regions of the world. An example of a country in Eastern Europe for which there are no detailed surveys at the NUTS-2 level or lower, is Poland, a country with an area of 312.696 km^2 and a population of over 38 million (as of December 31, 2017 according to the Central Statistical Office). Almost 90% of electricity is produced from conventional thermal sources. This is the fourth highest result in the European Union (data from 2017 [38]). In addition, taking into account the growing demand for electricity both from HH and the entire economy, it should be noted that energy policy is an important component of the Polish economy. Models estimating electricity consumption in a selected area of the country may constitute a tool supporting market analysis. The limited number of studies for Poland and other Central European countries is a potential obstacle towards sustainable development that needs to be redressed.

An aim of this study was to verify empirically the possibility of using nighttime light images for modeling the electricity consumption of voivodships in Poland on an annual basis (in accordance with the NUTS-2 division in force until December 31, 2017). This required, among others, the development of an appropriate set of independent variables based on images acquired over many years. In order to build the model, artificial neural networks (ANNs) were used. As a result, it was possible to develop non-linear models with automatically selected parameters.

Forecasts based on nighttime light images may give an opportunity to estimate energy consumption in areas where there is no or lack of access to statistical or system data. For Poland, satellite images are available more than six months before the official data provided by the Central Statistical Office. For current analyses of the energy market, the possibility of earlier estimation of energy consumption, both in total and divided into sectors of the economy, is undoubtedly highly desirable.

2. Principles of Artificial Neural Networks

ANNs were created in an attempt to imitate thought processes occurring in living organisms. They form a structure of connected nerve cells. The current definition of a single neuron was presented by McCulloch and Pitts in 1943 [39]. Fig. 2 shows a diagram of an artificial nerve cell. Numerous analogies with the biological model are visible. Inputs numbered x_1 to x_n are responsible for the introduction of signals into the cell and are the equivalent of dendrites. Weights marked w_1 to w_n in the figure are real numbers. Each x_i input is connected with a w_i weight. Signals entered into a cell are multiplied by the weight assigned to a given input. Therefore, network response depends on their value. In the learning process, the values of weights are modified in such a way that the network response becomes more precise. The discussed products of the values of the input signals and weights are added and then transformed by the so-

[1] Searching for publication titles and abstracts, the following keywords were used in a Scopus query: TITLE-ABS-KEY((energy OR electricity) AND (consumption OR demand OR usage) AND ("neural network*" OR "artificial intelligence" OR AI OR perceptron) AND ("nighttime image*" OR "night-time image*" OR "night time image*" OR "night-time light*" OR "nighttime light*" OR "night time light*" OR "night satellite imagery" OR "night light satellite imagery" OR (("satellite imagery") AND ("at night*")) OR linescan OR "DMSP*OLS" OR VIIRS OR "Day*Night" OR DNB)) and the equivalent WoS query. Scopus yielded one workshop proceedings. A thorough analysis of 19 publications found, showed that only one [35] concerns the analysis of data from DMSP/OLS, while the applied research methods did not use tools from AI.

The final version is available on the journal website at https://doi.org/10.1016/j.energy.2019.04.221

called activation function. To a certain extent, this is the equivalent of the biological nucleus of a cell. The resulting value leaves the cell with an output marked as *y*. This is the equivalent of a biological structure called axon.

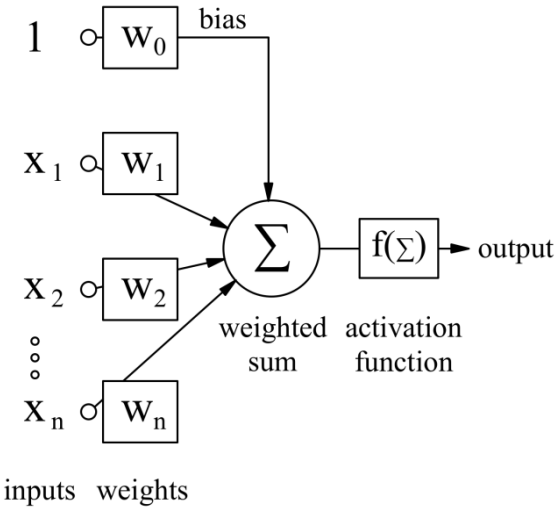

Fig. 2. Neuron diagram.

There are many types of ANNs, differing in the direction of signal flow, used learning algorithm and neuron definition. The multilayer perceptron (MLP) was used in this study. This is a network in which neurons are grouped into three types of layers: a single input layer, an output layer and at least one hidden layer between them (see [40]). Fig. 3 shows the MLP diagram with one hidden layer. Signals flow in one direction (from input to output). The neurons of the hidden and output layers take an active part in the learning process (their weights are modified). The cells grouped into the input layer do not gain any knowledge and have a technical function consisting mainly of disseminating model input signals among the neurons of the first hidden layer.

The MLP is an example of a supervised network. This means that there is a sub-program called the teacher, which is responsible for the ANN training process. Its task is to check the error generated by the network during the learning process in response to input data, and then to modify weights in such a way as to reduce the error generated by the ANN. The multiple presentation of the network of input and output patterns combined with weight correction leads to the asymptotic reduction of error to zero. This process carries the risk of the phenomenon of network overtraining, which denotes that learning responds to memory coupled with the loss of the ability to generalize knowledge. In order to prevent this situation and to ensure the proper development of the training process, it is necessary to build appropriate data sets. In practice, three subsets are used: training, validation and testing. The first – as the name suggests – is used to learn ANN. The second – validation – is usually randomly selected and excluded from the training set. Typically, it is smaller in number and used to determine the moment in which the learning process stops. If the total model error for data from the validation set starts to increase, the further modification of weights should be interrupted, as otherwise it will trigger the overlearning effect. Fig. 4 shows the model error for data from the training and validation sets as a function of the epoch (i.e. a single presentation of all data from the set).

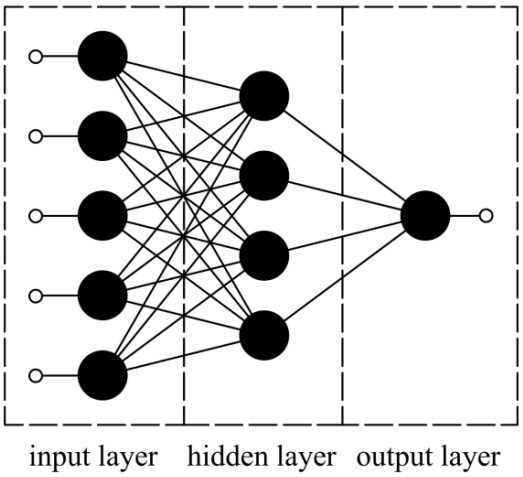

Fig. 3. MLP diagram.

The purpose of the test set is to check the quality of the trained ANN operation. It should be noted that in the literature the nomenclature of subsets – in particular validation and test – is not consistent. What is more, sometimes they are even named inversely. This should be taken into account, in particular, when conducting a literature review.

ANNs are now widely used in energy markets (see [41]). In particular, they are used in the forecasting (on the basis of system and meteorological data) of electricity prices (see MLP – [42,43,44]; MLP and pre-processing data using discrete cosine transforms – [45]; Probability Neural Network (PNN) – [46]; Radial Basis Function (RBF) Network – [47]); demand and

The final version is available on the journal website at https://doi.org/10.1016/j.energy.2019.04.221

consumption (see MLP – [48,49,50,51,52,53,54,55]; Recurrent Neural Networks (RNN) – [56]). In this paper, ANNs based on nighttime light images were used for modeling electricity consumption.

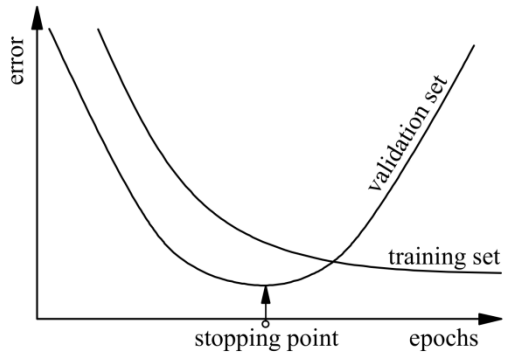

Fig. 4. Error during teaching ANN in supervised mode.

ANNs were used in the study due to their ability to model complex, nonlinear relations between independent and dependent variables. Based on Kolmogorov's theorem, it was shown that MLPs with two hidden layers and an appropriate number of neurons have the potential to model a polynomial of any degree (see [57]). In this paper, a network with only one hidden layer was used because, as the initial empirical comparative research carried out by the author showed, these networks were characterized by lower error rates than networks with a greater number of hidden layers. The reason for this situation cannot be fully explained. It should be assumed that it is related to the currently used training algorithms, which are not always able to exploit fully the greater potential of networks with a greater number of learning layers. It should be noted that the phenomenon described does not concern only the research in question and that it is common in ANN-based models.

3. Methodology

The empirical research required the development of a model determining the amount of electricity consumed per year at NUTS-2 level, i.e. in regions of Poland. The amounts of electricity consumed by: (i) the total economy, (ii) HH, ware used as the dependent variables (both sets of data were obtained from the Central Statistical Office). This means that it was necessary to create a model that worked for relatively small areas. Building a set of dependent variables required obtaining satellite data. Satellite images from 2013–2016 that showed average radiance composite images using nighttime data from the VIIRS DNB, and which were preliminarily processed by removing stray light, lightning, lunar illumination and cloud cover, were used in the research. NOE/NOAA stores images including radiance values that have undergone the stray-light correction procedure (see [58]) but not for the entirety of the period in question, while their resolution is lower than that of images used in this study. Chen and Nordhaus [59] emphasize that the pixel ground footprint of VIIRS images is 45 times smaller than the DMSP/OLS footprint, which in their opinion favors the use of the first in analyses covering small areas. It should be noted, however, that overpass time of the DMPS/OLS occurred approximately between 20:30 and 21:30, which corresponds more to the activity time of HH (especially for visible radiation) than the VIIRS' overpass time around 01:30 (detailed overpass times for a specific day can be found at https://ncc.nesdis.noaa.gov). As the model is expected to be workable in the future, it is assumed that only currently recorded images from the VIIRS DNB should be used.

As images of annual average radiation were not available for the entire period, it was necessary to introduce a uniform method for its determination using averaged images from individual months. For the area in question, nighttime light images were available only for the first and last three months of each year. Due to seasonal differences in brightness (related, among others, to changes in surface reflectivity caused by snow and vegetation cover, as observed by Levin [60], Levin and Zhang [61] – see Fig. 6), it was necessary to include the same months for all years in the analysis. These images may have contained lights from auroras, fires, boats and other temporal lights. The applied averaging procedure, however, had reduced to some extent their potential impact on the model's performance. Additionally, images from VIIRS in relation to DMSP-OLS, according to Elvidge et al. [58], are characterized by: vast reduction of the pixel footprint (ground instantaneous field of view – GIFOV), uniform GIFOV from nadir to edge of scan, lower detection limits, wider dynamic range, finer quantization and in-flight calibration. The last feature means that, at least to a certain extent, the need for calibration as related to the use of data from different

The final version is available on the journal website at https://doi.org/10.1016/j.energy.2019.04.221

sensors is eliminated (see [62]). Fig. 5 presents a fragment of the original Geo Tagged Image File Format (GeoTIFF) for December 2016, obtained from EOG resources, that shows an image of the entire country (Poland) and, separately, of all regions. It should be noted that where single images or full coverage of the analyzed area are lacking (which was not the case in this study), the presented procedure may be supplemented by patching the missing data. The method to address this was developed by Zhao et al. [3].

Fig. 5. Nighttime light image of Poland (left) and individual voivodships (right) for December 2016.
Source: Author's elaboration based on images from NOE/NOAA.

The averaged values were determined as the arithmetic mean, of pixel numbers for the months of January to March and October to December of the same calendar year, categorized according to brightness range. For that purpose, GeoTIFF images were converted into comma-separated values (CSV) text files including the coordinates of each pixel and a value representing brightness originally scaled from 0 to 255. The annual average values were determined using the software developed by the author of this study. A total of 64 images were received for four years. For all of them, the number of points was determined, which due to the represented brightness were classified into one of eight ranges: (i) 1–31, (ii) 32–63, (iii) 64–95, (iv) 96–127, (v) 128–159, (vi) 160–191, (vii) 192–223, (viii) 224–255 (see Fig. 6). The zero value was not included in range (i) because it represents an area with radiance below the minimum detectable level. Table 1 shows the average data for 16 voivodships calculated on the basis of six images and the classification of each of the pixels into one of eight brightness classes (sample data for 2016). The set of independent variables was supplemented with information from the year the averaged images originated.

For each year, the images were divided into 16 regions (voivodships). The QGIS application was used for this purpose. In total, 384 images were obtained.

Total radiation (SOL) for each voivodship was calculated using Eq. (2).

One of the factors strongly positively correlated with energy consumption is the total usable floor area of a dwelling. Fig. 7 and Fig. 8 show this dependence for 16 regions for total electricity consumption and electricity consumed by HH respectively. Diagrams cover the years 2013, 2014 and 2016. The year 2015 was not included due to lack of data from the Central Statistical Office. In real-world analyses, in addition to the incompleteness of data sets, another problem is the time of their creation. In practice, data on total usable floor area of dwellings is not available for periods earlier than those applicable to electricity consumption data. Thus, it is not possible to use them in the forecasting model. For this reason, it was necessary to use additional satellite images, which may to some extent replace inaccessible data and thus contribute to the improvement of the accuracy of ANN.

Therefore, it is appropriate to add an additional indicator to the model in order to determine the type of spatial development. One such indicator is the Normalized Difference Vegetation Index (NDVI). Its calculation is possible by means of formula Eq. (4).

$$NDVI = (NIR - RED)/(NIR + RED) \quad (4)$$

where:
NIR – near-infrared wavelength
RED – red wavelength

The study used a 16-day MODIS 250 m NDVI (MYD13Q1) acquired from Land Processes Distributed Active Archive Center [63]. For each year, images from the month of July were used. The mosaic command from SeaDAS was used to obtain one image covering the whole country. Then, in the QGIS application, fragments corresponding to the analyzed regions were identified. As built-up areas are particularly important from the point of view of electricity demand, an attempt was made on the basis of NDVI values to determine the number of pixels representing this type of spatial development. The procedure of cut-off thresholds, described in Taufik et

The final version is available on the journal website at https://doi.org/10.1016/j.energy.2019.04.221

al. [64], was applied. This approach often does not provide reliable information on built-up areas. For this reason, Land Cover Type Yearly Global 500 m Band 1 images, containing the global vegetation classification scheme defined in the International Geosphere-Biosphere Programme (IGBP) [65], were used interchangeably. The input variable (BU) was the number of pixels of the analyzed area representing zones classified as urban and built-up (value 13).

To a certain extent, this approach allowed for taking into account the existence of rural areas without nightlight. Their existence was indicated for Beijing and Hebei in Lu and Liu [66].

The quality of ANN performance was compared with results obtained using linear regressions.

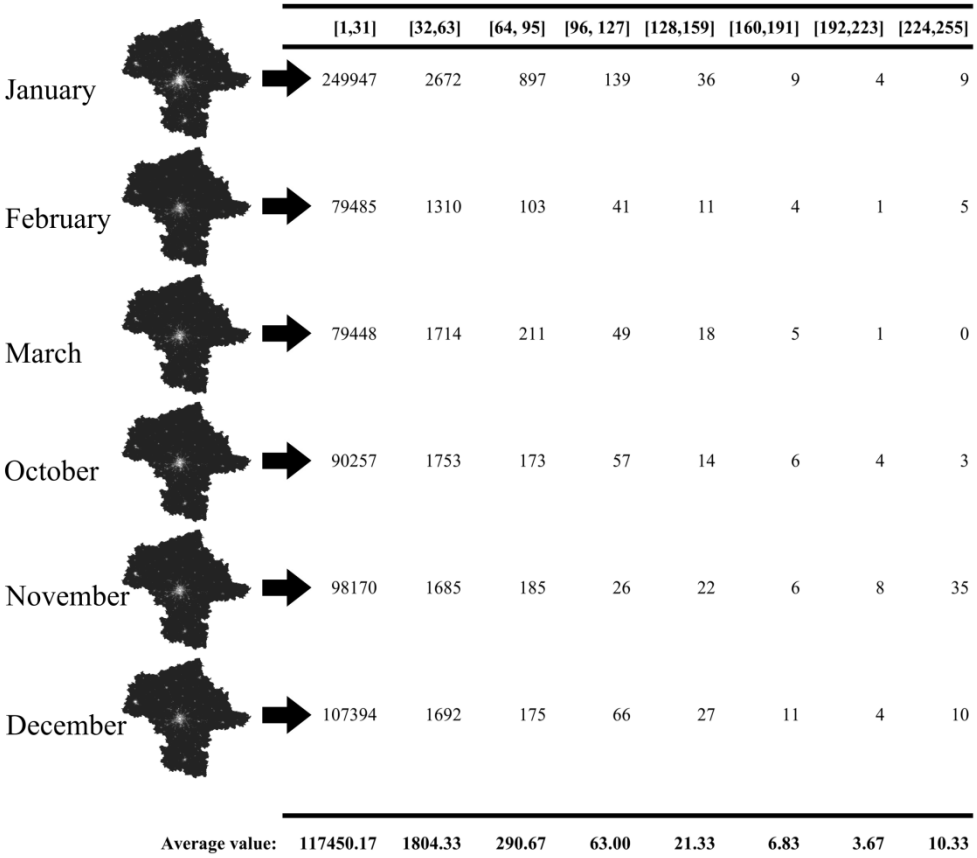

	[1,31]	[32,63]	[64, 95]	[96, 127]	[128,159]	[160,191]	[192,223]	[224,255]
January	249947	2672	897	139	36	9	4	9
February	79485	1310	103	41	11	4	1	5
March	79448	1714	211	49	18	5	1	0
October	90257	1753	173	57	14	6	4	3
November	98170	1685	185	26	22	6	8	35
December	107394	1692	175	66	27	11	4	10
Average value:	**117450.17**	**1804.33**	**290.67**	**63.00**	**21.33**	**6.83**	**3.67**	**10.33**

Fig. 6. Example of determination of the arithmetic averages of pixel numbers for the months of January to March and October to December of the same calendar year, categorized in eight brightness ranges for the Mazovian Voivodship (2016).

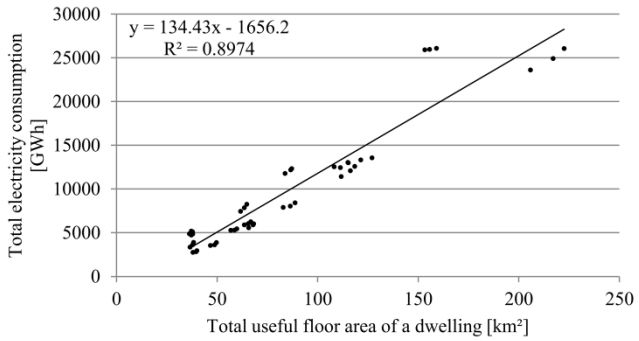

Fig. 7. Scatter diagram of total electricity consumption and total usable floor area of a dwelling (16 regions for years 2013–2016).

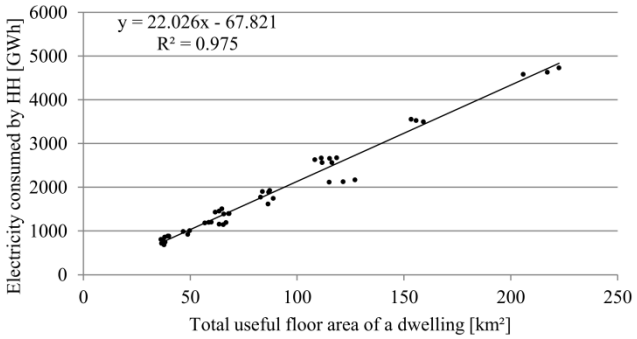

Fig. 8. Scatter diagram of electricity consumed by HH and total usable floor area of a dwelling (16 regions for years 2013–2016).

The final version is available on the journal website at https://doi.org/10.1016/j.energy.2019.04.221

As the number of 64 images is relatively small, it was decided to use the K-Fold Cross Validation. From the initial set of all images, 16 images were randomly selected to form a test set (the rest were used as training and validation data). Next, out of the remaining 48 images, 16 were randomly selected to form another test set. Repeating the above procedure led to the creation of four sets of data, for each of which the test set consisted of different cases (the product of any two different test sets is an empty set). This approach makes it possible to reduce, to a certain extent, the risk of obtaining unreliable results due to the limited number of cases.

Table 1
Averaged pixel numbers in eight brightness ranges for 16 regions in 2016

Region	Averaged pixel numbers of brightness according to range after scaling							
	[1,31]	[32,63]	[64,95]	[96,127]	[128,159]	[160,191]	[192,223]	[224,255]
Lower Silesia	73339.00	845.17	142.83	36.17	10.00	4.00	1.67	3.83
Kuyavian-Pomeranian	58013.17	463.00	42.50	9.33	4.33	1.67	0.50	0.83
Lublin	47449.00	533.33	100.67	25.33	4.17	1.83	1.50	16.67
Lubusz	32273.50	191.17	8.67	1.17	0.67	0.17	0.00	0.00
Łódź	60244.83	701.00	101.50	13.83	2.17	0.67	0.33	2.50
Lesser Poland	71708.33	706.83	66.00	6.67	2.17	1.00	0.17	4.83
Mazovian	117450.17	1804.33	290.67	63.00	21.33	6.83	3.67	10.33
Opole	30656.50	164.17	25.33	5.50	0.83	0.00	0.00	0.00
Subcarpathian	36576.67	338.17	40.00	3.33	1.33	1.17	0.00	10.33
Podlaskie	38144.33	214.00	30.83	4.50	1.00	0.00	0.00	0.00
Pomeranian	52244.83	926.67	114.00	18.83	6.33	1.67	1.67	1.67
Silesian	67009.50	1376.67	105.83	14.83	9.50	6.17	3.50	25.17
Świętokrzyskie	38718.67	211.33	27.17	2.00	0.50	0.33	0.00	0.00
Warmian-Masurian	49174.33	226.67	21.67	2.33	0.17	0.00	0.00	0.00
Greater Poland	110889.33	996.67	164.33	62.50	18.33	7.00	6.67	14.33
West Pomeranian	43530.33	362.00	49.00	8.17	1.67	0.33	0.50	5.67

3.1. Set of input variables and ANN parameters

Eight variants of independent variables presented in Table 2 were used in the ANN model tests.

Sets 1, 2, 5 and 7 differ from 3, 4, 6 and 8 respectively in the lack of a variable in the form of the number of pixels with the lowest value range. Its elimination can be compared by way of simplification (by analogy) to the use of a cut-off point in Eq. (3).

The number of neurons in the input layer for technical reasons had to be equal to the number of independent variables listed in Table 2. Selection of the number of neurons in the hidden layer and activation function in both learning layers was carried out experimentally. The search for the optimal number of cells was carried out in the ranges from 4 to 12 according to the algorithm shown in Fig. 9. This procedure was repeated successively for different learning algorithms: (i) the Broyden-Fletcher-Goldfarb-Shanno (BFGS), (ii) back propagation (momentum version with different values of learning coefficients and momentum), (iii) conjugate gradient.

Table 2
Sets of ANN input variables

No.	Independent variables
1	$p_{32,63}$; $p_{64,95}$; $p_{96,127}$; $p_{128,159}$; $p_{160,191}$; $p_{192,223}$; $p_{224,255}$
2	$p_{32,63}$; $p_{64,95}$; $p_{96,127}$; $p_{128,159}$; $p_{160,191}$; $p_{192,223}$; $p_{224,255}$; *SOL*
3	$p_{1,31}$; $p_{32,63}$; $p_{64,95}$; $p_{96,127}$; $p_{128,159}$; $p_{160,191}$; $p_{192,223}$; $p_{224,255}$
4	$p_{1,31}$; $p_{32,63}$; $p_{64,95}$; $p_{96,127}$; $p_{128,159}$; $p_{160,191}$; $p_{192,223}$; $p_{224,255}$; *SOL*
5	$p_{32,63}$; $p_{64,95}$; $p_{96,127}$; $p_{128,159}$; $p_{160,191}$; $p_{192,223}$; $p_{224,255}$; *SOL ; NDVI*
6	$p_{1,31}$; $p_{32,63}$; $p_{64,95}$; $p_{96,127}$; $p_{128,159}$; $p_{160,191}$; $p_{192,223}$; $p_{224,255}$; *SOL ; NDVI*
7	$p_{32,63}$; $p_{64,95}$; $p_{96,127}$; $p_{128,159}$; $p_{160,191}$; $p_{192,223}$; $p_{224,255}$; *SOL ; BU*
8	$p_{1,31}$; $p_{32,63}$; $p_{64,95}$; $p_{96,127}$; $p_{128,159}$; $p_{160,191}$; $p_{192,223}$; $p_{224,255}$; *SOL, BU*

$p_{i,j}$ – number of pixels in the range [i,j]

4. Comparative models

Three versions of linear regression were used as reference models for both total electricity consumption and energy consumed by HH.

The final version is available on the journal website at https://doi.org/10.1016/j.energy.2019.04.221

The first was regression of one variable (Reg. 1). SOL was used as an independent variable.

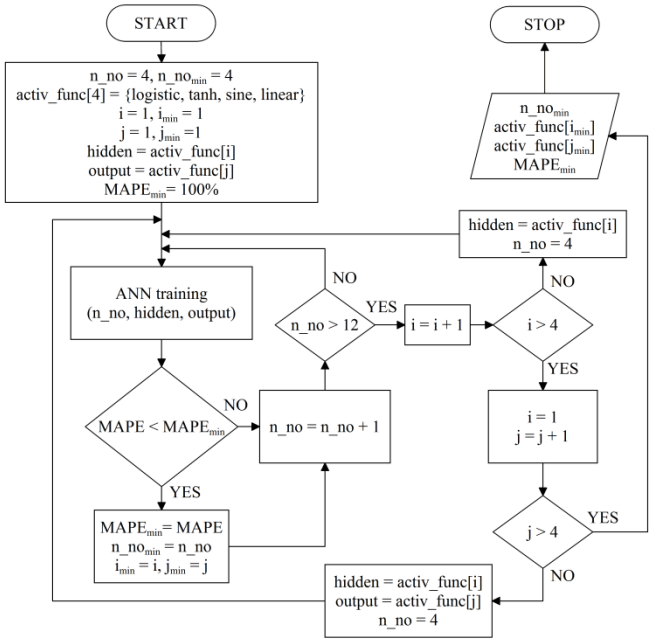

Fig. 9. Algorithm for selection of the best ANN.

The second regression (Reg. 2) was used to check whether the newly developed independent variables can be used not only in ANN, but also in linear models. In applied multiple regression as independent variables, the set of variables no. 3 (see Table 2) was assumed to be used.

Table 3
VIF values for potential independent variables

Variable[1)]	VIF values in subsequent calculation steps[2)]		
	I	II	III
***p*1,31**	3.2016	3.0902	3.0899
***p*32,63**	10.9069	10.5409	4.1896
*p*64,95	25.8585	**24.3197**	
***p*96,127**	23.1500	17.9616	5.0556
*p*128,159	**43.0968**		
***p*160,191**	19.1697	6.4830	6.4495
***p*192,223**	8.6088	8.5650	7.9775
***p*224,255**	2.5573	2.2576	2.2314

1) Bold font indicates variables with a final VIF value below 10.
2) Bold font indicates the maximum VIF value in the calculation step.

Table 4
p-values for independent variables (Reg. 2)

Variable	Dataset	Total electricity consumption					Electricity consumed by HH				
		p-values in subsequent calculation steps									
		I	II	III	IV	V	I	II	III	IV	V
$p_{1,31}$	I	0.7525	**0.7812**				0.0016	0.0015	0.0008	0.0005	
$p_{32,63}$		0.0000	0.0000	0.0000	0.0000	0.0000	0.0000	0.0000	0.0000	0.0000	
$p_{96,127}$		0.0031	0.0007	0.0006	0.0000	0.0000	0.0185	0.0044	0.0001	0.0001	
$p_{160,191}$		0.5619	0.5624	0.0933	**0.1017**		0.3209	**0.3237**			
$p_{192,223}$		0.2375	0.1137	**0.5209**			0.3575	0.1552	**0.2963**		
$p_{224,255}$		**0.8253**					**0.6483**				
$p_{1,31}$	II	0.1320	0.1209	**0.2149**			0.0003	0.0000	0.0000		
$p_{32,63}$		0.0000	0.0000	0.0000	0.0000	0.0000	0.0000	0.0000	0.0000		
$p_{96,127}$		0.1647	0.1306	0.0008	0.0010	0.0005	0.6802	**0.6237**			
$p_{160,191}$		**0.9318**					0.2416	0.1615	0.0060		
$p_{192,223}$		0.3735	**0.3254**				**0.9344**				
$p_{224,255}$		0.0950	0.0863	0.1456	**0.1540**		0.0803	0.0420	0.0085		
$p_{1,31}$	III	0.2515	0.1544	0.1477	**0.1788**		0.0000	0.0000	0.0000	0.0000	
$p_{32,63}$		0.0000	0.0000	0.0000	0.0000	0.0000	0.0000	0.0000	0.0000	0.0000	
$p_{96,127}$		0.0011	0.0009	0.0000	0.0000	0.0000	0.0232	0.0036	0.0005	0.0001	
$p_{160,191}$		0.7996	**0.6761**				**0.6886**				
$p_{192,223}$		**0.8502**					0.6589	**0.7831**			
$p_{224,255}$		0.4508	0.3338	**0.2047**			0.2543	0.2600	**0.1058**		
$p_{1,31}$	IV	0.5351	**0.5293**				0.0530	0.0479	0.0791	**0.1379**	
$p_{32,63}$		0.0000	0.0000	0.0000	0.0000		0.0000	0.0000	0.0000	0.0000	0.0000
$p_{96,127}$		0.0333	0.0069	0.0015	0.0019		0.4960	0.2867	**0.3109**		
$p_{160,191}$		**0.9953**					**0.8068**				
$p_{192,223}$		0.3026	0.2088	**0.2619**			0.1876	0.1485	0.0225	0.0207	0.0103
$p_{224,255}$		0.0763	0.0713	0.0289	0.0029		0.3222	**0.3266**			

p-values to four decimal places; the largest *p*-value in a given calculation step is indicated in bold font.

The final version is available on the journal website at https://doi.org/10.1016/j.energy.2019.04.221

The Variance Inflation Factors (VIF) were calculated for each of the new variables according to Eq. (5). The aim was to eliminate from the model those input variables which are characterized by too high a degree of correlations and associations with the remaining variables. The obtained VIF values are presented in Table 3.

$$VIF_k = 1/(1 - R_k^2) \quad (5)$$

where: R_k^2 – the R^2-value obtained by regressing the k-th explanatory variable on the remaining explanatory variables.

It was assumed that a variable for which the VIF value exceeded 10 to the highest degree should be removed from the model and the VIF value for a new, reduced set of independent variables was re-calculated. On this basis, two variables were removed from the model: $p_{64,95}$ and $p_{128,159}$. Further elimination of variables took place, due to p-values, separately for each of the four used sets of independent variables. As before, it was assumed that in each calculation step, one input variable of p-value exceeding 0.05 to the highest degree should be eliminated. The obtained results are presented in Table 4.

Table 5
Number of neurons in three layers

	ANN 1	ANN 2	ANN 3	ANN 4	ANN 5	ANN 6	ANN 7	ANN 8
	Forecasts of total electricity consumption							
no. of neurons	7-6-1	8-7-1	8-9-1	9-10-1	9-7-1	10-7-1	9-7-1	10-7-1
	Forecasts of electricity consumed by HH							
no. of neurons	7-5-1	8-5-1	8-8-1	9-6-1	9-5-1	10-5-1	9-5-1	10-5-1

The third variant (Reg. 3) was a multiple regression with eight independent variables as in set no. 3 (see Table 2). As the p-value analysis would lead to elimination of a significant number of variables and, consequently, to the creation of a model highly similar to model 2, it was decided to ignore very high p-values and introduce eight variables into the model in an unchanged form.

4. Results

More than 150,000 networks with MLP architecture were tested. Out of 64 images, 42 constituted a training set (65.63% of cases), 6 a validation set (9.37% of data) and 16 a test set (25.00% of cases). As only one dependent variable was modeled at all times, the networks had a single neuron in the output layer. The number of neurons in the input layer was adjusted (equal) to the number of independent variables.

Table 5 provides a summary of the number of neurons from which the best ANNs modeling total electricity consumption and electricity consumed by HH at regional level were built. In all networks a hyperbolic tangent (in the hidden layer) and logistic (in the output layer) were used as activation functions. ANNs were trained using the Broyden-Fletcher-Goldfarb-Shanno algorithm (BFGS). Table 6 contains MAPEs for the best ANNs and three versions of linear regression (for each test set). In all cases ANN was clearly better than linear regression. The model that was characterized by the lowest MAPE value for the data being a sum of four 16-element test sets (created using the K-Fold Cross Validation) was network no. 2. Fig. 10 and Fig. 11 show scatter diagrams of the obtained results from the actual values, corresponding to the test set by the best MLPs for total electricity consumption and electricity consumption by HH respectively.

The largest forecast error for total electricity consumption (observation marked with an arrow in Fig. 10) was made for Łódź Voivodship in 2013 and amounted to 6247 GWh. For this Voivodship in the brightness range [128–159], there were definitely more pixels (44) than in other cases included in the training set. In the entire data set, a similarly high number of pixels in the above mentioned range occurred only for the Mazovian Voivodship in 2013, which was also randomly qualified to the test set. It should be assumed that the discussed model error is closely related to the lack of cases with a similar number of pixels in the brightness range [128–159] in the training set.

The final version is available on the journal website at https://doi.org/10.1016/j.energy.2019.04.221

Table 6
MAPEs for test data

Dataset	Model										
	ANN 1	ANN 2	ANN 3	ANN 4	ANN 5	ANN 6	ANN 7	ANN 8	Reg. 1	Reg. 2	Reg. 3
	Total electricity consumption										
Total	16.48	15.49	17.37	16.72	16.20	16.39	12.31	**11.95**	25.51	28.65	29.62
I	18.25	14.89	16.00	13.96	14.65	**12.14**	12.89	13.77	25.59	32.63	33.11
II	**9.59**	16.25	15.89	17.01	17.52	18.13	12.28	11.91	26.04	26.40	32.51
III	12.42	12.59	14.56	12.80	14.66	15.39	10.92	**10.80**	21.63	23.60	18.99
IV	25.68	18.23	23.04	23.12	17.97	19.90	13.15	**11.34**	28.80	31.97	33.88
	Electricity consumed by HH										
Total	12.04	8.69	11.80	9.51	10.22	9.17	8.13	**7.92**	15.43	19.75	17.25
I	14.66	**7.71**	16.69	11.44	11.67	9.38	10.38	9.64	18.26	22.08	21.32
II	8.16	5.88	7.50	7.04	7.83	7.83	5.83	**5.43**	12.22	15.13	15.92
III	**7.74**	10.14	10.85	8.91	8.79	9.55	8.70	8.80	14.79	15.79	14.98
IV	17.61	11.06	12.14	10.65	12.58	9.92	**7.60**	7.82	16.47	26.00	16.78

The smallest MAPE values for a given test set are marked in bold font.

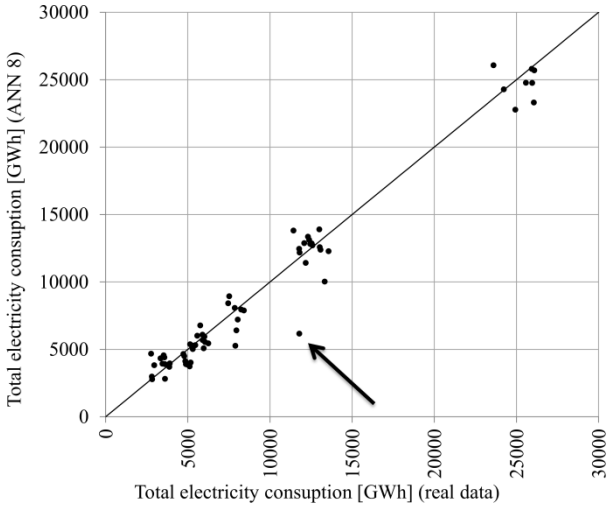

Fig. 10. Scatter diagram for total electricity consumption (ANN 2, testing dataset).

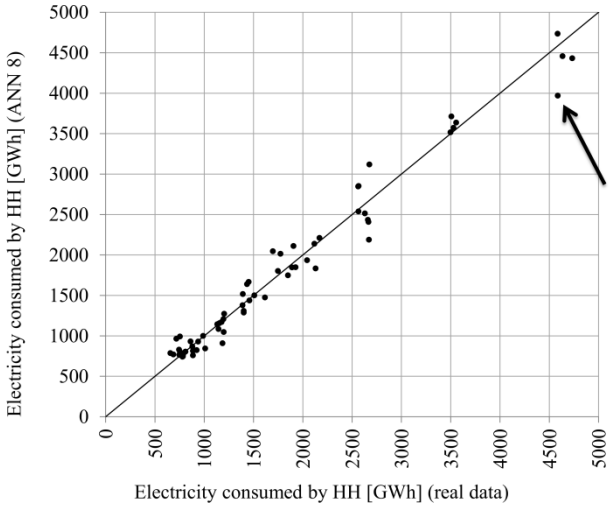

Fig. 11 Scatter diagram for electricity consumption by HH (ANN 2, testing dataset).

A similar situation (the same voivodship) occurred in modeling the electricity consumed by HH (model error 907 GWh, observation marked with an arrow in Fig. 11).

MLPs with the lowest total MAPE (ANN 8) have been used to model total electricity consumption in Slovakia. This Central European country borders Poland. Its administrative division covers eight regions, whose average area is 6,129 km^2 and is more than three times smaller than the average area of regions in Poland (19,543 km^2). Slovakia has a 10% lower average population density and smaller regional variation, ranging from 68 to 136 inhabitants per km^2, while in Poland it ranges from 59 to 369 inhabitants per km^2. Slovakia also has a different economic structure than Poland. The case study of Slovakia has provided verification that the ANN 8 model could be successfully applied in other areas, different in economic and demographic terms. Data on electricity consumption were obtained from the Statistical Office of the Slovak Republic. MAPE for the forecast of total electricity consumption was 13.86%.

5. Conclusions

Research has shown that it is possible to determine the amount of electricity consumed on the basis of satellite nighttime light images. Models based on AI in the form of ANN are able to determine the amount of electricity used both in total and by selected economy sectors (on the example of HH). ANN modeling of total electricity consumption was characterized by

The final version is available on the journal website at https://doi.org/10.1016/j.energy.2019.04.221

much higher error for the test set than for networks modeling electricity consumption by HH. It should be assumed that this is due to the closer relation between the amount of visible radiation emitted and the electricity consumed by HH. This is confirmed by analogous results obtained by the reference linear regression model (Reg. 1 – see Table 6).

Extending the set of independent variables by the number of pixels of brightness between 1 and 31 for the total test set resulting from the application of K-Fold Cross Validation translated into improvement in the quality of obtained results only in combination with BU. For three out of eight 16-element test sets, this led to the network (ANN 8) obtaining results with a lower MAPE value. The use of the SOL variable in the model resulted in ANN 2 and 4 obtaining the lowest values of error meter (for the entire test set) for both total electricity consumption and electricity consumed by HH.

The best network (ANN 8) for Polish regions was achieved for two types of surveyed output variables MAPEs of 11.95% and 7.92% respectively. These values are 13.56% and 7.51% lower than the results of the best linear regression model (see Table 6).

Satisfactory results were also achieved in the case of the Slovak regions (MAPE of 13.86% for total electricity consumption). This indicates the model's ability to operate (even without optimizing its structure) in different areas under varying economic and demographic conditions.

This confirms the appropriateness of using non-linear methods to associate nighttime light images with electricity consumption.

It should be emphasized that among the independent variables there was no information that would clearly enable the identification of each voivodship. Thus, the ANNs were forced to model the dependent variable only on the basis of the brightness of the pixels in the satellite images, without the possibility to refer to electricity consumption in a given voivodship in another year, which was the case for a training set. This increases the objectivity of the research and indicates the potential of networks for modeling additional regions to those used for ANNs training.

The limitations of the tests carried out should be noted. These are mainly due to the amount of available data. In the course of the analyses, data were available for only four years. In modeling 16 regions, this translated to 64 cases, 42 of which were used for a training set. This number is much smaller than the desired size of a training set. It is not possible to extend the data back to earlier years due to the lack of satellite images, nor is it feasible to include more recent data (e.g. for 2017) due to the lack of electricity consumption data (from the Energy Market Agency JSC made available by the Central Statistical Office). A solution to this problem could be to extend the area of research to other countries. An increase in the number of cases would enable the application of other types of ANN, including networks with a greater number of hidden layers, the so-called deep neural networks (deep learning) [67]. It should be taken into account, however, that there may be differences in the relations between nighttime lights and electricity consumption resulting e.g. from different household habits, different levels of use of electrical equipment (including heating) and different economic characteristics (as confirmed by the studies of Xie and Weng [21]). It is also possible to seek the improvement of the quality performance of the described model in a different structure of training data, in particular at a later stage of the study, where the differentiation of the brightness ranges of the pixels in the satellite images should be considered. Consideration should also be given to the modification of the procedure for averaging the number of pixels over a given brightness range on an annual basis. However, accurate identification and elimination from the calculation of averages of images characterized by nighttime lights of unusual brightness should be covered by the study.

Acknowledgements

The author thanks the anonymous reviewers whose comments and suggestions were very helpful in improving the quality of this paper. The author also thanks the editor for their constructive suggestions.

Appendix A. Supplementary data

Supplementary data to this article can be found in file Appendix_A.csv.

References

[1] Ghosh T, Anderson SJ, Elvidge CD, Sutton PC. Using night-time satellite imagery as a proxy measure of human well-being. Sustain 2013;5:4988–5019. https://doi.org/10.3390/su5124988.

[2] Keola S, Andersson M, Hall O. Monitoring economic development from space: using nighttime light and land cover data to measure economic growth. World Dev 2015;66:322–34. https://doi.org/10.1016/j.worlddev.2014.08.017.

[3] Zhao N, Hsu F-C, Cao G, Samson EL. Improving accuracy of economic estimations with VIIRS DNB image products. Int J Remote Sens 2017;38(21):5899–918. https://doi.org/10.1080/01431161.2017.1331060.

[4] Sutton PC, Costanza R. Global estimates of market and non-market values derived from nighttime satellite imagery, land cover, and ecosystem service valuation. Ecol Econ 2002;41:509–27. https://doi.org/10.1016/S0921-8009(02)00097-6.

[5] Zhao N, Liu Y, Cao G, Samson EL, Zhang J. Forecasting China's GDP at the pixel level using nighttime lights time series and population images. GISci & Remote Sens 2017;54(3):407–25. https://doi.org/10.1080/15481603.2016.1276705.

[6] Zhu X, Ma M, Yang H, Ge W. Modeling the spatiotemporal dynamics of gross domestic product in China using extended temporal coverage nighttime light data. Remote Sens 2017;9:626. https://doi.org/10.3390/rs9060626.

[7] Marx A, Rogers MZ. Analysis of Panamanian DMSP/OLS nightlights corroborates suspicions of inaccurate fiscal data: A natural experiment examining the accuracy of GDP data. Remote Sens Appl: Soc Environ 2017;8:99–104. https://doi.org/10.1016/j.rsase.2017.08.005.

[8] Wang W, Cheng H, Zhang L. Poverty assessment using DMSP/OLS night-time light satellite imagery at a provincial scale in China. Adv Space Res 2012;49:1253–64. https://doi.org/10.1016/j.asr.2012.01.025.

[9] Ma T, Zhou C, Pei T, Haynie S, Fan J. Quantitative estimation of urbanization dynamics using time series of DMSP/OLS nighttime light data: A comparative case study from China's cities. Remote Sens Environ 2012;124:99–107. https://doi.org/10.1016/j.rse.2012.04.018.

[10] Wang L, Wang S, Zhou Y, Liu W, Hou Y, Zhu J, Wang F, Mapping population density in China between 1990 and 2010 using remote sensing. Remote Sens Environ 2018;210:269–81. https://doi.org/10.1016/j.rse.2018.03.007.

[11] Kumar P, Sajjad H, Joshi PK, Elvidge CD, Rehman S, Chaudhary BS, Tripathy BR, Singh J, Pipal G. Modeling the luminous intensity of Beijing, China using DMSP-OLS night-time lights series data for estimating population density. Phys Chem Earth, Parts A/B/C 2018;(In Press, Corrected Proof). https://doi.org/10.1016/j.pce.2018.06.002.

[12] Tan M, Li X, Li S, Xin L, Wang X, Li Q, Li W, Li Y, Xiang W. Modeling population density based on nighttime light images and land use data in China. Appl Geogr 2018;90:239–47. https://doi.org/10.1016/j.apgeog.2017.12.012.

[13] Stathakis D, Baltas P. Seasonal population estimates based on night-time lights. Comput, Environ Urban Syst 2018;68:133–41. https://doi.org/10.1016/j.compenvurbsys.2017.12.001.

[14] Huang Q, Yang X, Gao B, Yang Y, Zhao Y. Application of DMSP/OLS night-time light images: a meta-analysis and a systematic literature review. Remote Sens 2014;6:6844–66. https://doi.org/10.3390/rs6086844.

[15] Addison D, Stewart B. Nighttime lights revisited. The use of nighttime lights data as a proxy for economic variables. The World Bank Policy Res Work Pap 2015;7496.

[16] de Miguel AS, Zamorano J, Castaño JG, Pascual S. Evolution of the energy consumed by street lighting in Spain estimated with DMSP-OLS data. J Quant Spectrosc & Radiat Transf 2014;139:109–17. https://doi.org/10.1016/j.jqsrt.2013.11.017.

[17] Rossi F, Bonamente E, Nicolini A, Anderini E, Cotana F. A carbon footprint and energy consumption assessment methodologyfor UHI-affected lighting systems in built areas. Energy Build 2016;114:96–103. https://doi.org/10.1016/j.enbuild.2015.04.054.

[18] To W-M, Lee PKC, Lai T-M. Modeling of monthly residential and commercial electricity consumption using nonlinear eeasonal models — the case of Hong Kong. Energies 2017;10:885. https://doi.org/10.3390/en10070885.

[19] De Lauretis S, Ghersi F, Cayla J-M. Energy consumption and activity patterns: An analysis extended to total time and energy use for French households. Appl Energy 2017;206:634–48. https://doi.org/10.1016/j.apenergy.2017.08.180.

[20] Hu S, Yan D, Guo S, Cui Y, Dong B. A survey on energy consumption and energy usage behavior of households and residential building in urban China. Energy Build 2017;148:366–78. https://doi.org/10.1016/j.enbuild.2017.03.064.

[21] Tripathy BR, Sajjad H, Elvidge CD, Ting Y, Pandey PC, Rani M, et al. Modeling of electric demand for sustainable energy and management in India using spatio-temporal DMSP-OLS night-time data. Environ Manage 2018;61:615–23. https://doi.org/10.1007/s00267-017-0978-1.

[22] Xie Y, Weng Q. World energy consumption pattern as revealed by DMSP-OLS nighttime light imagery. GISci & Remote Sens 2016;53(2):265–82. https://doi.org/10.1080/15481603.2015.1124488.

[23] Shi K, Chen Y, Yu B, Xu T, Yang C, Li L, et al. Detecting spatiotemporal dynamics of global electric power consumption using DMSP-OLS nighttime stable light data. Appl Energy 2016;184:450–63. https://doi.org/10.1016/j.apenergy.2016.10.032.

[24] Shi K, Yu B, Huang C, Wu J, Sun X. Exploring spatiotemporal patterns of electric power consumption in countries along the Belt and Road. Energy 2018;150:847–59. https://doi.org/10.1016/j.energy.2018.03.020.

[25] Elvidge CD, Baugh KE, Kihn EA, Kroehl HW, Davis ER, Davis CW. Relation between satellite observed visible-near infrared emissions, population, economic activity and electric power consumption. Int J Remote Sens 1997;18(6):1373–9. https://doi.org/10.1080/014311697218485.

[26] He C, Ma Q, Liu Z, Zhang Q. Modeling the spatiotemporal dynamics of electric power consumption in Mainland China using saturation-corrected DMSP/OLS nighttime stable light

data. Int J Digit Earth 2014;7(12):993–1014. https://doi.org/10.1080/17538947.2013.822026.

[27] Xie Y, Weng Q. Detecting urban-scale dynamics of electricity consumption at Chinese cities using time-series DMSP-OLS (Defense Meteorological Satellite Program-Operational Linescan System) nighttime light imageries. Energy 2016;100:177–89. https://doi.org/10.1016/j.energy.2016.01.058.

[28] Ramdani F, Setiani P. Multiscale assessment of progress of electrification in Indonesia based on brightness level derived from nighttime satellite imagery. Environ Monit & Assess 2017;189(6):249. https://doi.org/10.1007/s10661-017-5949-8.

[29] Doll CNH, Muller J-P, Morley JG. Mapping regional economic activity from night-time light satellite imagery. Ecol Econ 2006;57:75–92. https://doi.org/10.1016/j.ecolecon.2005.03.007.

[30] Letu H, Nakajima TY, Nishio F. Regional-scale estimation of electric power and power plant CO2 emissions using Defense Meteorological Satellite Program Operational Linescan System nighttime satellite data. Environ Sci & Technol Lett 2014;1:259–65. https://doi.org/10.1021/ez500093s.

[31] Shi K, Yu B, Huang Y, Hu Y, Yin B, Chen Z, Chen L, Wu J. Evaluating the Ability of NPP-VIIRS Nighttime Light Data to Estimate the Gross Domestic Product and the Electric Power Consumption of China at Multiple Scales: A Comparison with DMSP-OLS Data. Remote Sens 2014;6:1705–24. https://doi.org/10.3390/rs6021705.

[32] Fehrer D, Krarti M. Spatial distribution of building energy use in the United States through satellite imagery of the earth at night. Build Environ 2018;142:252–64. https://doi.org/10.1016/j.buildenv.2018.06.033.

[33] Li C, Li G, Zhu Y, Ge Y, Kung H, Wu Y. A likelihood-based spatial statistical transformation model (LBSSTM) of regional economic development using DMSP/OLS time-series nighttime light imagery. Spatial Stat 2017;21:421–39. https://doi.org/10.1016/10.1016/j.spasta.2017.03.004.

[34] Jing X, Shao X, Cao C, Fu X, Yan L. Comparison between the Suomi-NPP day-night band and DMSP-OLS for correlating socio-economic variables at the provincial level in China. Remote Sens. 2016;8(1):17. https://doi.org/10.3390/rs8010017.

[35] Reza SSO, Chasovskich VP. Monitoring of the human activities from DMSP/OLS nighttime imageries. CEUR Workshop Proceedings 2018;2131:1.

[36] Wang J, Aegerter C, Xu X, Szykman JJ. Potential application of VIIRS Day/Night Band for monitoring nighttime surface PM2.5 air quality from space. Atmospheric Environ 2016;124:55–63. https://doi.org/10.1016/j.atmosenv.2015.11.013.

[37] Fu D, Xia X, Duan M, Zhang X, Li X, Wang J, Liu J. Mapping nighttime PM2.5 from VIIRS DNB using a linear mixed-effect model. Atmospheric Environ 2018;178:214–22. https://doi.org/10.1016/j.atmosenv.2018.02.001.

[38] EUROSTAT. Electricity generation statistics – first results, https://ec.europa.eu/eurostat/statistics-explained/index.php?title=Electricity_generation_statistics_–_first_results; 2018 [accessed 24 March 2019].

[39] McCulloch S, Pitts W. A logical calculus of the ideas immanent in nervous activity. Bull Math Biophys 1943;5:115–33. https://doi.org/10.1007/BF02478259.

[40] Rosenblatt F. The perceptron: A probabilistic model for information storage and organization in the brain. Psychol Rev 1958;65(6):386–408. https://doi.org/10.1037/h0042519.

[41] Weron R. Electricity price forecasting: a review of the state-of-the-art with a look into the future. Int J Forecast 2014;30:1030–81. https://doi.org/10.1016/j.eneco.2017.06.020.

[42] Gareta R, Romeo LM, Gil A. Forecasting of electricity prices with neural networks. Energy Convers Manage 2006;47:1770–8. https://doi.org/10.1016/j.enconman.2005.10.010.

[43] Keles D, Scelle J, Paraschiv F, Fichtner W. Extended forecast methods for day-ahead electricity spot prices applying artificial neural networks. Appl Energy 2016;162:218–30. https://doi.org/10.1016/j.apenergy.2015.09.087.

[44] Mirakyan A, Meyer-Renschhausen M, Koch A. Composite forecasting approach, application for next-day electricity price forecasting. Energy Econ 2017;66:228–37. https://doi.org/10.1016/j.eneco.2017.06.020.

[45] Anbazhagan S, Kumarappan N. Day-ahead deregulated electricity market price forecasting using neural network input featured by DCT. Energy Convers Manage 2014;78:711–9. https://doi.org/10.1016/j.enconman.2013.11.031.

[46] Lin W-M, Gow H-J, Tsai M-T. Electricity price forecasting using Enhanced Probability Neural Network. Energy Convers Manage 2010;51(12):2707–14. https://doi.org/10.1016/j.enconman.2010.06.006.

[47] dos Santos Coelho L, Santos AAP. RBF neural network model with GARCH errors: Application to electricity price forecasting. Electr Power Syst Res 2011;81:74–83. https://doi.org/10.1016/j.epsr.2010.07.015.

[48] Geem ZW, Roper WE. Energy demand estimation of South Korea using artificial neural network. Energy Policy 2009;37:4049–54. https://doi.org/10.1016/j.enpol.2009.04.049.

[49] Ekonomou L. Greek long-term energy consumption prediction using artificial neural networks. Energy 2010;35:512–7. https://doi.org/10.1016/j.energy.2009.10.018.

[50] Jasiński T. Prediction of electricity demand with artificial neural networks – an example of the Ontario province in Canada and the Italian market. In: Brotas L, Roaf S, Nicol F, editors. Design to Thrive, PLEA 2017 Conference Proceedings Volume I, Edinburgh: NCEUB; 2017, p. 1414–21.

[51] Kialashaki A, Reisel JR. Modeling of the energy demand of the residential sector in the United States using regression models and artificial neural networks. Appl Energy 2013;108:271–80. https://doi.org/10.1016/j.apenergy.2013.03.034.

[52] Kialashaki A, Reisel JR. Development and validation of artificial neural network models of the energy demand in the industrial sector of the United States. Energy 2014;76:749–60. https://doi.org/10.1016/j.energy.2014.08.072.

[53] Muralitharan K, Sakthivel R, Vishnuvarthan R. Neural network based optimization approach for energy demand prediction in smart grid. Neurocomputing 2018;273:199–208. https://doi.org/10.1016/j.neucom.2017.08.017.

[54] Pino-Mejías R, Pérez-Fargallo A, Rubio-Bellido C, Pulido-Arcas JA. Comparison of linear regression and artificial neural networks models to predict heating and cooling energy demand, energy consumption and CO2 emissions. Energy 2017;118:24–36. https://doi.org/10.1016/j.energy.2016.12.022.

[55] Yokoyama R, Wakui T, Satake R. Prediction of energy demands using neural network with model identification by global optimization. Energy Convers Manage 2009;50:319–27. https://doi.org/10.1016/j.enconman.2008.09.017.

[56] Ruiz LGB, Rueda R, Cuéllar MP, Pegalajar MC. Energy consumption forecasting based on Elman neural networks with evolutive optimization. Expert Syst With Appl 2018;92:380–9. https://doi.org/10.1016/j.eswa.2017.09.059.

[57] Kůrková V. Kolmogorov's theorem and multilayer neural networks. Neural Netw 1992;5:501–6. https://doi.org/10.1016/0893-6080(92)90012-8.

[58] Elvidge DC, Baugh K, Zhizhin M, Hsu FC, Ghosh T. VIIRS night-time lights. Int J Remote Sens 2017;38(21):5860–79. https://doi.org/10.1080/01431161.2017.1342050.

[59] Chen X, Nordhaus W. A test of the new VIIRS lights data set: population and economic output in Africa. Remote Sens 2015;7:4937–47. https://doi.org/10.3390/rs70404937.

[60] Levin N. The impact of seasonal changes on observed nighttime brightness from 2014 to 2015 monthly VIIRS DNB composites. Remote Sens Environ 2017;193:150–64. https://doi.org/10.1016/j.rse.2017.03.003.

[61] Levin N, Zhang Q. A global analysis of factors controlling VIIRS nighttime light levels from densely populated areas. Remote Sens Environ 2017;190:366–82. https://doi.org/10.1016/j.rse.2017.01.006.

[62] Li X, Zhou Y. A stepwise calibration of global DMSP/OLS stable nighttime light data (1992–2013). Remote Sens 2017;9:637. https://doi.org/10.3390/rs9060637. ISSN 20724292.

[dataset] [63] Didan K.. MYD13Q1 MODIS/Aqua Vegetation Indices 16-Day L3 Global 250m SIN Grid V006. 2015, distributed by NASA EOSDIS LP DAAC, https://doi.org/10.5067/MODIS/MYD13Q1.006.

[64] Taufik A, Ahmad SSS, Ahmad A. Classification of Landsat 8 satellite data using NDVI thresholds. J Telecommun, Electron Comput Eng. 2016;8(4):37–40.

[dataset] [65] Friedl M, Sulla-Menashe D. MCD12Q1 MODIS/Terra+Aqua Land Cover Type Yearly L3 Global 500m SIN Grid V006. 2015, distributed by NASA EOSDIS Land Processes DAAC, https://doi.org/10.5067/MODIS/MCD12Q1.006.

[66] Lu H, Liu G. Spatial effects of carbon dioxide emissions from residential energy consumption: A county-level study using enhanced nocturnal lighting. Appl Energy 2014;131 :297–306. https://doi.org/10.1016/j.apenergy.2014.06.036.

[67] Schmidhuber J. Deep learning in neural networks: An overview. Neural Netw 2015;61:85–117. https://doi.org/10.1016/j.neunet.2014.09.003.